Applied Energy 178 (2016) 43–55

Contents lists available at ScienceDirect

Applied Energy

journal homepage: www.elsevier.com/locate/apenergy

Investigation of thermal control for different SOFC flow geometries

Mahshid Fardadi [a], Dustin F. McLarty [b], Faryar Jabbari [a,*]

[a] Department of Mechanical and Aerospace Engineering, University of California, Irvine, CA 92697, United States
[b] School of Mechanical and Materials Engineering, Washington State University, Pullman, WA 99164-2920, United States

HIGHLIGHTS

- Thermal control of cross flow SOFC is investigated.
- Changing flow directions in a subset of channels can improve thermal profiles.
- Non uniform air flow improves thermal profile at the expense of small efficiency loss.
- Advanced controllers minimize thermal variations for large changes in power demand.

ARTICLE INFO

Article history:
Received 25 February 2016
Received in revised form 9 May 2016
Accepted 9 June 2016
Available online 16 June 2016

Keywords:
Cross-flow SOFC
Thermal control
Channel flow reversal
Nonuniform air flow

ABSTRACT

A dynamic solid oxide fuel cell (SOFC) model is used to investigate the effects of different flow arrangements, as well as those of non-uniform air flow across channels, on temperature profile and thermal gradients under transient and steady state response. A high performance multi-input multi-output feedback controller has been developed to minimize SOFC spatial temperature variations during changes in power demands for different flow patterns. Numerical results show that the controller would result in negligible temperature variations for the modified cross-flow arrangement proposed here, even for large changes in the power drawn. The combination of a high performance controller and design modification results in a more uniform temperature profile at steady state nominal conditions, and modest variations in temperature profile, from the nominal, for ±15% change in power. Similarly, non-uniform air flow rate decreases the temperature gradient as well as maximum temperature across the cell, though its effect is less pronounced in the closed loop response.

1. Introduction

Distributed energy resources (DER), particularly dispatchable generation, is a potentially disruptive technology which is receiving increasing attention [1–5]. Advances in the smart grid infrastructure has enabled additional DER deployment strategies, and distributed generation is seen as the future of the smart grid [6]. The widespread deployment of solar and wind generation, combined with the high cost of installing new transmission capacity, has resulted in periods of intermittent congestion which require energy storage or dispatchable resources to resolve [7,8]. Niche applications which require ultra-high reliability or power quality have turned to on-site power generation in tandem with grid power in order to reduce down-time [9]. Reliability is also a concern for critical infrastructure during severe weather events [10]. Distributed generation can also serve as alternative to the unreliable or non-existent electric power infrastructure in the developing world [11].

High temperature fuel cell systems are an attractive solution with ultra-low pollutant emissions and high efficiency. Many systems in production today are fuel flexible, using suitable high methane content biogas, digester gases and landfill gases to produce power with little or no impact on performance or emissions, after appropriate gas clean-up process [12–14]. While the initial markets for stationary fuel cells has primarily been base-load generation, often with heat recovery, the majority of distributed generation applications will require responsive capabilities. Some of the dynamics a fuel cell may need to respond to include: a rapidly changing building load, stochastic charging of electric vehicles, intermittent cloud cover impacting a local solar array, or a sudden fuel transition between biogas and pipeline gas.

Solid oxide fuel cell (SOFC) systems are being commercialized for these applications by a variety of industrial concerns. Significant challenges arise in making SOFC systems responsive. Advanced integrated system controls, as explored in [15–23], are necessary in order to maintain system integrity, durability, and

* Corresponding author at: Department of Mechanical and Aerospace Engineering, University of California, Irvine, Irvine, CA 92697, United States.
E-mail address: fjabbari@uci.edu (F. Jabbari).

http://dx.doi.org/10.1016/j.apenergy.2016.06.015
0306-2619/

Nomenclature

w(t)	vector of exogenous inputs (e.g., external disturbances and reference inputs)	δu	change in control inputs from the steady state values
u(t)	vector of control inputs	δz	change in control variables from the steady state values
z(t)	vector of control variables	δw	change in disturbances from the steady state values
y(t)	measurement vector (sensors)	u_{ref}	control inputs at steady state nominal conditions
δx	change in states from the steady state values	y_{ref}	measurement vector at steady state nominal conditions
δy	change in sensors from the steady state values	w_{ref}	disturbance vector at steady state nominal conditions
		z_{ref}	control variables at steady state nominal conditions

lifespan. Controller design is highly dependent upon the application requirements and system configuration, but generally thermal response should be damped to the extent possible, given the materials used and the high temperatures involved. This paper explores several methods to mitigate temperature deviations through channel routing design, flow rate control, and inlet temperature control.

Thermal management within an SOFC is accomplished primarily by controlling the bulk air flow rate to the cathode. A natural temperature gradient develops as the air flows across the heat generating cell. The temperature throughout the SOFC must be maintained within specific bounds which ensure sufficient electrochemical activity without excessive degradation. These boundary specifications dictate the overall temperature gradient which can be sustained. Higher localized temperature gradients are also undesirable due to the associated thermal stress which can lead to failure in the ceramic cells. Co-flow, counter-flow, and cross-flow are the three most frequently studied arrangements for planar SOFC. Co-flow design, in which the fuel and air travel across the cell in the same direction, has the most uniform temperature profile among the three arrangements [24]. The counter-flow configuration in which air and fuel travel in opposite directions has the highest efficiency and higher local temperature gradients [25–27]. Finally, cross-flow design, in which the paths of air and fuel channels are perpendicular to each other, often yields significant manufacturing benefits in the manifold design and gas routing of the system. However, cross-flow often has the worst temperature profile (e.g., maximum temperature across the cell and local gradients) [28,29].

Typically, increased bulk air flow can be used to reduce temperature gradients and thermal stress [16,23,30–33], but additional air flow comes with costs. The primary cost is the power requirement of a blower needed to push the additional air through the system. A typical blower may utilize as much as 15% of the total electric generated by the SOFC [34,35]. The secondary cost is pre-heating the inlet air to as much as 1023 K, requiring efficient and expensive heat exchangers and mixing mechanisms. Additionally, increased cathode air flow dilutes the exhaust stream lowering the temperature and the potential for heat recovery. Several stack configurations and fuel cell thermal management strategies have been discussed in the literature (as examples, see [28,36–39]).

Responsive SOFC systems will not only be impacted by design choices for the steady-state temperature profile, but also by transient responses and off base-load power production. Nakajo et al. [40,41] showed that the probability of failure significantly increases due to temperature variations during transients. Inui et al. [42] demonstrated a broad power range could be achieved while operating within the temperature bounds by manipulating both cathode air flow and inlet temperature. The latter work is based primarily on steady state analysis and is not directly related to the transient operation under changing loads or disturbances. Zhang et al. [25], analyzed the steady-state temperature distribution for both counter-flow and cross-flow geometries using a two dimensional mathematical model. Their results indicate a preference for counter-flow due to the higher efficiency of the cell, and lower exiting temperature of the cathode stream. The higher efficiency largely stems from the higher average temperature of the positive electrode–electrolyte–negative electrode (PEN) assembly.

Bavarian and Soroush [43,44] developed a mathematical model of a proton-conducting solid oxide fuel cell (SOFC) and analyzed its steady state behavior as well as the effects of the operating conditions, such as convection heat transfer coefficient and inlet fuel and air temperatures, on the steady state behavior.

Christman and Jensen [45] numerically analyzed four aspects of SOFC rib geometry (e.g. shape, spacing, and surface area). Surface roughness was shown to improve fuel cell performance, by increasing active surface area, with limited adverse thermal effects. Geometry and flow modifications may thus be more mechanically stable than monolithic, or mono-block-layer-built (MOLB), cells which exhibit sharp thermal gradients.

Recknagle et al. develop a three-dimensional model for co-flow, counter-flow and cross-flow planar SOFC [46]. These models were investigated using the same flow rates with variable flow temperatures. The authors find that, for a given average cell temperature and similar fuel utilization, co-flow case has the most uniform temperature distribution and the smallest thermal gradient.

Chen et al. [47] showed that a planar modular short SOFC stack is advantageous for establishing a high power supply. They also optimized combinations of alternative manifold arrangements for both the fuel and air flow paths, in counter flow fuel cells.

Razbani et al. [48] developed an experimental set-up for a cross flow type stack of six cells to measure the temperature distribution, in steady state conditions. They investigated the effects of fuel utilization and excess air on the location of maximum temperature.

Yuan and Liu [29] investigated the effects of non-uniform air and fuel flow distributions for a cross-flow cell. A progressively decreasing air inlet flow profile, along the row of channels, results in peak temperatures rising by 10%, while a progressively increasing air flow profile reduces peak temperature by 6%. In this paper we observe similar trends and further investigate the benefits of non-uniform air flow distribution, by increasing the air flow in the regions of peak temperature, near the fuel inlet.

Iwata et al. [49] developed a numerical approach for estimating temperature and current density profiles of a planar-type SOFC unit with co, counter, and cross-flow configurations. They investigated operating pressure, gas recirculation ratio, and physical property effects on current and temperature distributions. They showed that with adiabatic boundary conditions, in co-flow case, temperature increases along the flow direction and the temperature profile has a maximum near the fuel inlet in the counter-flow case.

ŞEN in [28] developed a full CFD (computational fluid dynamics) model and showed that under the same operating condition and voltage, changing the flow directions (e.g. variety of options such as L-Shape channels) results in a more uniform open loop

temperature profile, though the study did not include closed loop operation.

Fardadi et al. investigated the ability to control spatial temperature variations under load perturbations for co-flow and counter-flow configurations [50,35,51–53]. It was shown that a centralized controller offers important advantages for the co-flow and counter-flow designs. Advanced control techniques were applied to minimize thermal variations across a significant range of power variations. They also addressed concerns that specific actuator limitations, namely the blower response dynamics, can be readily addressed with the incorporation of a dynamic blower model within the control system [35,51–53].

Here we combine a geometric design modification, along with the use of non-uniform air flow rate for different channels, to improve steady state and transient temperature profiles. This modified cross flow configuration results in a more uniform temperature profile (e.g., lower maximum temperature difference across the cell as well as lower local temperature gradient) for steady state condition. More importantly, it is also more controllable in the sense that the same control methodology results in higher performance, in the form of lower closed loop temperature variation during load perturbation.

The control technique used in co-flow and counter-flow papers was shown to be effective for those configurations in [50,35,51]. Due to the difficulties in cross-flow fuel cells (namely due to the challenging temperature profile), the technique was not as effective for the cross-flow configuration. This paper extends the control methodology of [35,51–53] and introduces additional design elements to address the cross-flow geometry SOFC, which may be more cost effective to manufacture. Previous studies demonstrated the non-uniform temperature distribution resulting from a cross-flow arrangement [28,29,46]. Addressing the uneven temperature distributions, and the resulting thermal stresses [29], is the objective of this study.

Cross-flow configuration, with relatively simply geometry, can offer significant manufacturing benefits in manifold design and gas routing of the system. However, it is often associated with large temperature differences across the cell and higher local temperature gradients compared with the co-flow and counter-flow designs. The modifications suggested in this paper address the thermal problems, with minimal additional complexity in manifolding, manufacturing or design.

There have been some attempts to use different flow patterns (i.e. [28]) to minimize temperature difference across the cell, and using progressively increasing/decreasing air flow rate (i.e. [29]) to reduce peak temperature in open loop system. Unlike [28,29], here we used thermal profile as a guide to determine the flow pattern and the required air flow rate for each channel. Furthermore, we show that combining the two approaches yields better open loop thermal response.

We use the thermal profile of the nominal system as the guide for the modifications made. For example, the flow directions in air or fuel channels are altered based on the location of hot/cold spots to better distribute electrochemical reaction and cooling air flow. Similarly, the air flow in channels containing high temperature regions is increased relative to the rest of the channels. In open loop operations, combining the two approach results in significantly lower temperature gradient as well as lower temperature difference across the cell at the expense of modest penalty in efficiency.

Our primary interest is to minimize closed loop temperature variations during load perturbation. The new flow patterns render the fuel cell more controllable, in the sense that the control methodology is more effective in minimizing temperature variations than in the nominal design. As a result, by relying on simple changes in the channel flow directions, significant thermal management and control is established, without the need for complex channel designs (and their corresponding manufacturing and cost concerns).

For the simulations presented here, a quasi-3D cross-flow SOFC model is used. The underlying methodology is similar to the ones used in some of the references above and, as a result, the modeling component is discussed only briefly. The interested reader can consult the appropriate references for all relevant detail. First, a baseline operating condition is established in order to evaluate the impact of changing flow directions and flow distribution. The thermal profiles of the co-flow, counter-flow and cross-flow designs are compared to show the thermal management challenge faced in the cross-flow case. Next, both open and closed loop transient temperature responses are evaluated for large fluctuations in power demand, for the cross-flow SOFC. Closed loop response was obtained with a high performance controller, initially designed relying on a linearized model, but applied to the full nonlinear model for all of the results shown. Finally, open and closed loop results are compared and discussed.

2. Background

2.1. Fuel cell stack

Here we present a brief summary discussing only key elements of the model that are related to the concepts discussed here. Full descriptions of these expressions can be found in published works [50,35,51–54]. The methodology used here has been previously used by others, including [18,32,33,36,40–42,55–58], who have compared predictions to both cell and system level experimental data [18,33,40,41,59,60]. The model used here is based on conservation of mass, species, and energy, as well as equations of convective and conductive heat transfer, steam reformation reactions, momentum, and fuel cell electrochemistry. This dynamic electrochemistry model is used to evaluate temperature control for cross-flow configuration, as well as co-flow and counter-flow cases.

A model developed by McLarty [54] leverages the matrix based computation of the Matlab® platform to efficiently compute the dynamic response of a spatially discretized fuel cell. The model is readily adapted to different geometries and flow configurations (i.e. co-flow, counter-flow or cross-flow) that are present in this study. The model has been compared with traditional modeling techniques and the results were qualitatively and quantitatively similar for co-flow and counter-flow configurations. The reduced computational burden permits the more refined spatial discretization necessary to capture the key characteristics of cross-flow (e.g. cold and hot spots).

For spatial and temporal resolution, the fuel cell is quasi-dimensionally discretized (in 3-D) into ten (or five) nodes along the flow directions. Each node consisting of 5 components, the anode current collector, fuel channel, positive electrode–electro lyte–negative electrode (PEN) assembly, oxidant channel, and cathode current collector control volumes as shown in Fig. 1. For

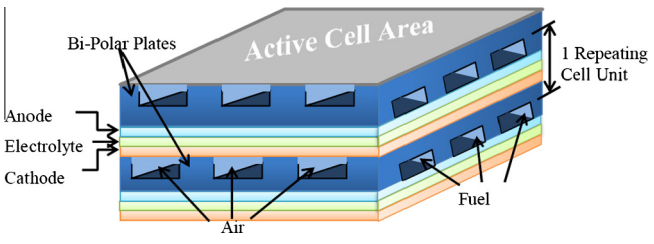

Fig. 1. Fuel cell stack repeating unit and control volume description [54].

the purposes of this study, initially a 10×10 spatial resolution is used to capture local variation in temperature and current in open loop system. McLarty [54] showed that the impact of additional discretization beyond 10 segments is minimal. For simplicity a 5×5 spatial resolution model was used for control design while limiting the number of states (model order). In the direction normal to the plane of the fuel cell a separate control volume represents each of the five components which together comprise a single repeating stack unit. The model includes heat transfer, energy conservation, reformation, momentum and electrochemistry terms for each of the 100 (for 10×10 nodes model) or 25 (for 5×5 nodes model) spatially arranged nodes to accurately determine local species concentrations, temperatures, reformation kinetics, and electrochemical activity (see [50,35,51–54]).

Within each node the states include: the temperature of all five control volumes, the mole fraction of six anode species (CH_4, CO, CO_2, H_2, H_2O, N_2,), two cathode species (N_2, O_2), molar flow rates of both the anode and cathode, and the electrochemical current. As a result, there are 16 dynamic equations (and thus states) for each node. The dynamic expressions used to capture the relevant physical phenomena at the timescale of interest in the dynamic simulation (i.e. greater than 10 ms) apply regardless of the flow geometry. The electrochemical kinetics and electric current flow dynamics are assumed to be sufficiently fast to be considered always at steady state. Finally, due to the very low Reynolds number (mid two figures) a full CFD model is not required.

3. Objective

The study aims to investigate the impact different flow arrangements may have on the spatial temperature distribution, specifically the peak temperature and the peak temperature gradient. This study further aims to evaluate the potential impact of controlled air flow perturbations to mitigate temperature fluctuations during transient response, e.g. power tracking. A previously studied co-flow SOFC with 100% external reformation, generating a net power of 3.5 kW, is used as the baseline. The air inlet temperature of (1021 K) and air flow rate of ($86 * 10^{-5}$ kmol/s) were determined to result in an average PEN temperature of 1073 K with an average temperature gradient of 10 K $cm^{-1}$for the baseline configuration. The same initial conditions for the baseline configuration such as air flow rate, air inlet temperature, fuel inlet temperature, fuel utilization and net power are used for counter and cross-flow arrangements, as well. Fig. 2 shows steady state temperature profile for co-flow, counter-flow and cross-flow configurations respectively. Nominal operating conditions are listed in Table 1 of the Appendix.

The PEN temperatures must be maintained above a minimum temperature to retain a sufficiently high current, while not exceeding a peak temperature threshold which results in accelerated degradation. Aguiar et al. [27,61], determined that the maximum allowable total temperature difference across the 10 cm cell is 100 K, and the maximum allowable temperature gradient is 10 K/cm. The gradient threshold scales inversely with the size of a cell. Commercial systems with substantially larger surface areas (1 m * 1 m) are subject to the chemical activity and degradation limits, but must be designed with substantially lower temperature gradients. The simulations here are based on a research cell (10 cm * 10 cm) for which a variety of data are available and can be used to evaluate design concepts. The flow design and control methods discussed here could be readily applied to mitigate temperature perturbations during transient response of larger commercial systems. Typically, a fuel cell stack is comprised of hundreds of cells, here for 3.5 kW power, we have one hundred cells stacked together.

As seen in Fig. 2, the traditional flow arrangement for cross-flow configuration results in the highest peak temperature and peak temperature gradient (maximum temperature difference across the cell), compared with co-flow and counter-flow configurations. Temperature difference across the cell peaks at 100 K, 68 K, and 124 K for co-flow, counter-flow, and cross-flow, respectively. Counter-flow has the lowest peak temperature but higher temperature gradient in the high activity region near the fuel entrance. In all cases, the overall temperature difference across the cell and local gradients increase significantly during power tracking transients. As discussed in [40,41,61], these lead to higher thermal fatigue and thus higher probability of failure and shorter lifetime. In the following, a number of alternative designs, aim at ameliorating this concern, are discussed. Effect of alternative flow arrangements as well as using non-uniform air flow rate, will also be discussed.

Changing the flow directions, for either air or fuel, can affect the overall thermal profile in a cross-flow FC (fuel cell). Fig. 3 shows schematics[1] of several possible flow patterns. Here for ease of presentation the schematics are sketched for the 5×5 nodes model. For 5×5 nodes model, channel 1 means first 20% of the width of cell from one side, channel 2 means 2nd 20% of the width (e.g. if the total width is 10 cm, channel 2 means from 2 cm to 4 cm from one side) and so on. For $10 * 10$ nodes similar patterns are used (e.g., every other one). In all schematics, the air flows in the vertical direction (in blue) and fuel flows in the horizontal direction (in red).

The arrangement in the left hand side of Fig. 3 is the cross-flow configuration (basic arrangement). The basic arrangement of cross-flow is highly desirable due to the low cost of manufacturing. Due to the high temperature gradient, as well as high maximum temperature difference across the cell, available commercial cross-flow arrangement leads to highly complicated and expensive design (e.g. serpentine design). Here we use a basic planar cross-flow design and consider modest design modification to reduce variations in the temperature across the cell. As in co-flow and counter-flow, temperature typically increases in the airflow direction of a cross-flow cell. However, the increase is non-uniform with a larger increase occurring near the center where electrochemical activity is high. To represent typical pre-reformed fuel, the fuel inlet flow used here contains 1% methane. Generally, the non-uniformity in temperature profile is more pronounced with methane in the fuel inlet since there is endothermic fuel reformation reaction near the inlet, further cooling the region near the inlet. It can be postulated that reversing the air (and/or fuel) flow in some of the channels might result in a more benign thermal profile. The alternative designs shown in Fig. 3 are among several alternatives studied. For brevity, only 2 are shown. Since here we have kept the air flow rate, air inlet temperature, fuel temperature, fuel utilization and power constant for all arrangements, any change in the fuel flow rate directly corresponds to a change in efficiency. Any further reference to a change in efficiency in this paper corresponds to a change in the fuel flow rate from that of the basic cross-flow arrangement.

The basic approach for alternative design is to send more air or cooler air to hotter regions. Similarly, reversing the direction of fuel in the highest temperature regions (often near the fuel inlet) could help cool the hot spots. A variety of options exist, but here for brevity we only show two, guided by this basic approach. Other alternatives were evaluated, but none was better, noticeably, than these two arrangements.

Direction 2, in the middle of Fig. 3, is developed by reversing flows in every other channel. This arrangement reduces maximum temperature difference across the cell and temperature gradients

[1] For interpretation of color in 'Fig. 3', the reader is referred to the web version of this article.

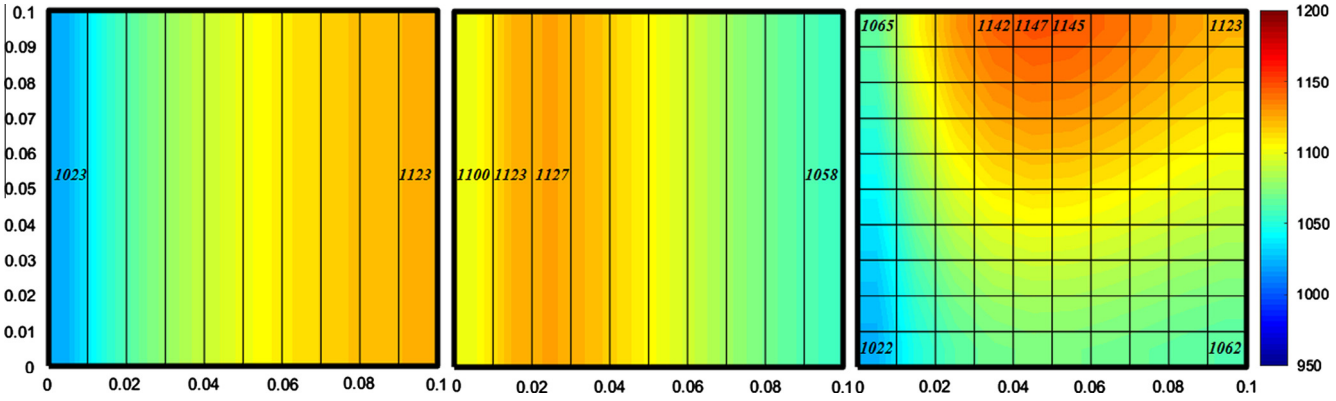

Fig. 2. Steady state nominal condition PEN temperature profile. Left: co-flow configuration. Middle: counter-flow configuration. Right: cross-flow configuration.

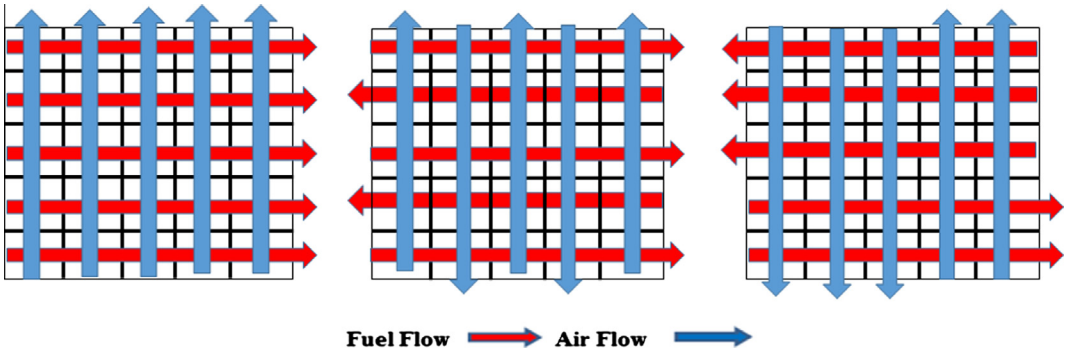

Fig. 3. Alternative flow arrangements: Top left: traditional cross-flow design (Direction 1). Top middle: Direction 2. Top right: modified cross-flow, Direction 3.

and results in modest increase in efficiency. However, it is likely that this arrangement creates challenges in the manufacturing process, particularly if the number of channels is high.

The idea for Direction 3, in the right side of Fig. 3, is to achieve a similar effect as the previous reversed channel configuration with the simplest flow manifolding possible. This is achieved with a single alternation of direction for both air and fuel flow, with channels in roughly the first half of the plate in the original direction and those in the second half reversed. In these simulations both 5 and 10 channels were used for both air and fuel, so for 5 channels the split is slightly uneven with the first 3 air flow channels (from left to right) reversed from the original direction and the last two channels unchanged. Similarly, for fuel flow, the first two (five for a 10 channels) channels (form bottom to top) remain unchanged from the original direction, while the last three (five for a 10 channels) channels reversed. The change in air flow from the basic cross-flow configuration raises the temperature in the lower left corner, while the change in fuel flow shifts a portion of the heat generation away from the hot area in the basic design. Direction 3 results in 48 K lower temperature difference across the cell than the basic cross-flow arrangement, and a net improvement in efficiency of 1.4%. Peak temperature gradients are also decreased by a modest 6 K/cm (Table 5 of Appendix).

The choice of flow direction is motived by the observation that temperatures increase primarily in the air flow direction, and peak temperatures occur in areas of high electrochemical activity. Different arrangements have varying impacts on leveling the thermal profile. For commercial applications manufacturing considerations are critical. Given that a stack typically contains a large number of cells, Designs 2 is, in all likelihood, more difficult to manufacture, while Design 3 offers a reasonable compromise of improved performance with minimal complexity. It should be noted that the 5×5 model is somewhat more coarse but the results are consistent with 10×10, showing the same trends albeit with minor difference in the exact values. The computation burden associated with control design with the 10×10 model is considerably higher and, as a result, we relied on the 5×5 model for the closed loop cases.

Another method to level the temperature profile is deployment of non-uniform flow rates between air channels. Again, the thermal profile with uniform flow provides a guideline for which channels should have higher and lower flow rates. Since the thermal profile for regular cross-flow is different from modified cross-flow configuration, the air flow ratio is also different for different arrangements. The highest amount of air flow rate is for the channel associated with the location of hot spot and lowest amount of air flow rate is entering the channel associate with the cold spot. Here the ratio between the highest and lowest amount of air flow rate is 3 to 1 for 10×10 nodes for both regular and modified cross-flow arrangements. Details for 5×5 nodes are specified in Table 4 of Appendix. The most passive means of differentiating the airflow is with different surface roughness. Different friction factor values were thus applied to the air channels. Non-uniform air flow decreases both peak temperature and temperature gradient for the basic cross-flow and the modified cross-flow configurations. Improvement in temperature profile and gradient in Direction 3 can also be met by simply using non uniform air flow rate in the original configuration. However, the latter approach requires more fuel flow resulting in lower efficiency, by approximately 3% which is not insignificant.

Of the arrangements discussed, as well as several other permutations, the most promising design was Direction 3. For brevity, the following control development will focus on Direction 3 (denoted as Modified Cross-flow) with uniform and non-uniform air flow rates in the rest of the paper.

4. Linearization, model reduction and control design

As in Fardadi et al. [50,35,51–53], we consider operation under nominal conditions, subjected to 15% changes in the power demand. To minimize the resulting thermal variations, we will design the controller with cathode inlet temperature and air flow rates as actuators (see [50,35,51–53] for a discussion on the choice of actuators). To this end, the spatially resolved nonlinear dynamic models are linearized, the order of the resulting models reduced and high performance controllers are designed using the reduced order linear models. These controllers are used to simulate the response of the full nonlinear models. Due to similarity with the developments in [50,35,51–53], we provide only a brief overview and emphasis the differences.

We need to design a separate controller for each configuration (regular and modified cross-flow with uniform and non-uniform air flow rate each, for a total of four). Therefore, we developed four models, two for the Basic cross-flow and two for the Modified cross-flow, each with uniform and non-uniform air flow. For simplicity, here we used a 5×5 nodes models for both regular and modified cross-flow for the purpose of control design. (The number of states in the 10 node model is 1600, complicating the control design without any noticeable improvement.) Each was linearized around its own nominal operating condition as specified in Table 2 of the Appendix. The inlet conditions (e.g. air flow rate, and air inlet temperature) are chosen to maintain an average electrolyte temperature of 1073 K with a temperature gradient of 10 K/cm across the 10 cm length of co-flow planar cell. The reduced order linear model and the complete nonlinear system model differed by less than 1 K in the open loop response to a 15% load change. Now consider the schematics of Fig. 4, representation standard control implementation (see Refs. [50,62,63], for example), where the box 'Plant' refers to the actual nonlinear model, with u_{ref}, y_{ref}, w_{ref}, and z_{ref} the inputs and outputs corresponding to the steady-state nominal conditions. Inputs u and w being set to u_{ref} and w_{ref} (set-point inputs) in the absence of disturbances, and the output will match y_{ref} and z_{ref}. As the disturbance is introduced the output will differ from y_{ref} and z_{ref}. The linearization about nominal operating condition results in an approximation of how the outputs differ from nominal values (i.e., δy and δz) due to δu and δw.

Deviation of the state, input, and output from their nominal trajectories are indicated by δx, δu, δw and δy. The resulting linear model is in form of Eq. (1) with the A, B_1, B_2, C_1, C_2, D_{11}, D_{12}, D_{21}, D_{22} matrices determined by the built-in Simulink/Matlab tools.

$$\begin{cases} \dot{\delta x} = A\delta x + B_1\delta w + B_2\delta u \\ \delta z = C_1\delta x + D_{11}\delta w + D_{12}\delta u \\ \delta y = C_2\delta x + D_{21}\delta w + D_{22}\delta u \end{cases} \quad (1)$$

Here, $w(t) \in R^{m_1}$ is a vector of exogenous inputs (e.g., external disturbances and reference, i.e., power drawn in this case), $u(t) \in R^{m_2}$ is the vector of control inputs (air flow rate and cathode inlet temperature), $y(t) \in R^{p_2}$ is the measurement vector (plate temperatures at various positions on the cell), and $z(t) \in R^{p_1}$ is a vector of control variables (variation from nominal temperatures at a number of points) .Variables with δ denote change from the nominal (baseline) values.The specific disturbances, actuators, and sensors are similar to those used for the co-flow and counter-flow configurations presented in Fardadi et al. [48–50,35] and listed in Table 3 of the Appendix. The control inputs of air flow rate (a measure of blower power) and cathode inlet temperature are readily manipulated. In [50,35,51,52] it was shown that the controller can suppress the non-minimum phase-like behavior of blower easily by adding the blower model to the fuel cell model for control development. Here we focus more on the design of the bipolar plate and the ability to control temperature variations during load perturbation. Consequently, for simplicity we used air flow rate directly as an actuator instead of blower power. The sensors have been selected based on practical considerations such as proximity and coupling with the key performance objective: reducing the temperature variations from the nominal profile along the fuel cell during transient operation. Since peak temperatures (and gradients) can move in two physical directions, depending on fuel composition and flow conditions, a relatively high number of sensors are needed.

Temperature sensors are the plate temperatures at various locations. Since PEN temperatures are not easily measurable, plate temperatures, which are in close proximity to the PEN and can more easily be measured, are used. Fuel flow rate is linearly related to current which is an indirect measure of heat generation in the fuel cell. As a result, we used a measurement of the current as additional sensed variables for the controller.

As mentioned earlier, we have total of 25 nodes and each node contains 16 states. Therefore, the full linearized model contains 400 states. The order of the model has to be reduced to reduce computational burden and sensitivity to numerical error. After removing uncontrollable and unobservable states the order of the model was reduced to 295. In the second step, the states with the least effect on the system response have been removed; this reduction is conducted by calculating the Hankel singular values [60] of the system, and keeping only those states with singular values greater than 10^{-4}. The resulting model has 36 states, and as with any model order reduction, they do not represent any physical entities. The open-loop response to the same 15% load transient remained within 1^{o}K of the full order linear model.

The controller is designed based on the H-infinity approach and the LMI toolbox of MATLAB [63], which was previously used in [50,35,51–53]. The controller aims to minimize fuel cell tempera-

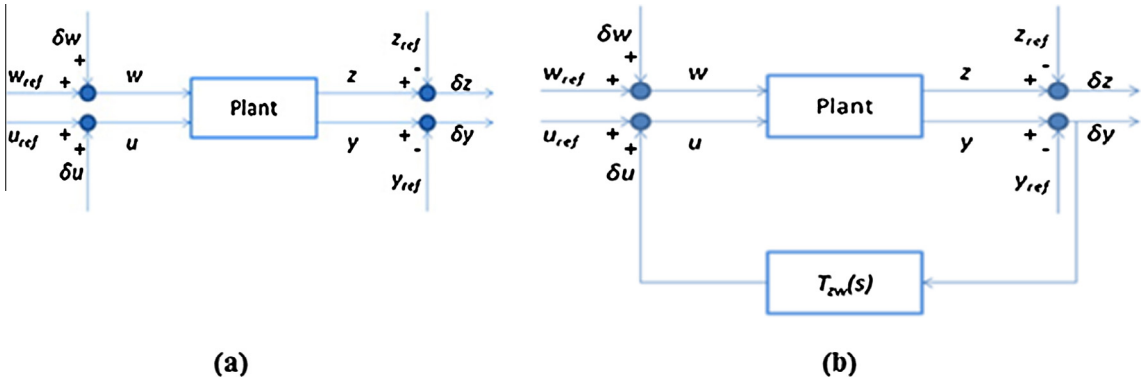

Fig. 4. (a) Linearization block diagram. (b) Feedback control block diagram [50,35,51–53].

ture variations from the nominal operating conditions, in response to the changes in the power demand. The reduced order linear model is used to obtain a compensator of the form:

$$\begin{cases} \dot{x}_c = A_c x_c + B_c \delta y \\ \delta u = C_c x_c + D_c \delta y \end{cases} \quad (2)$$

Here, A_c, B_c, etc. are the controllers matrices and Eq. (2) represents the dynamics of the controller which has the variations from the nominal temperatures as its input, to produce the control signal $u = \delta u + u_{ref}$. The goal of controller structure, a standard schematics of a closed loop system shown in right side of Fig. 4, is minimizing the effects of disturbance, e.g., changes in the power demand, or the fuel cell temperature variations from the nominal case. The controller has the same order as the plant (i.e., dim of A_c is the same as dim of A). In this figure T_{zw} is corresponding to compensator which has a transfer function form of Eq. (2). Refs. [62–66] contains all relevant details.

5. Results

5.1. Steady state nominal temperature profile for different flow arrangements

This section presents simulation results for the steady state nominal operating condition for cross-flow arrangement and the modified cross-flow. The simulations were conducted with the spatially resolved nonlinear models of a cross-flow SOFC (basic and the modified arrangements). Fig. 5 shows the simple basic cross-flow (left plots) and modified cross-flow (right plots) temperature profiles at steady state nominal operating conditions with uniform flow rate (top plots) and non-uniform flow rate (bottom plots).

In all cases, the profile is primarily affected by the air flow direction, with peak temperatures in areas of high local current density. The basic cross-flow configuration has air flowing from bottom to top, and fuel from left to right. The combination of relatively high hydrogen content and low Ohmic resistance results in a hot spot in the top center of the temperature profile. The modified cross-flow changes the air and fuel flow directions which result in a drastically different distribution of current density. Two areas of moderately high current density appear near both fuel entrances. This current distribution results in a more uniform temperature profile. Introducing non-uniform flow rates lessens the severity of the peak temperature and temperature gradients near the hot spots of both configurations, as seen in Fig. 5, which illustrates that the non-uniform air flow rate decreases significantly maximum temperature difference across the cell for the basic cross-flow arrangement (73 K instead of 124 K for the uniform air flow distribution), and modified cross-flow arrangement (49 K instead of 76 K for the uniform air flow rate). Non-uniform air flow rate also decrease the maximum temperature gradient compared to the uniform air flow rate in both the basic and the modified design.

5.2. Temperature profile for different flow arrangements under load perturbation

In this section, simulation results of basic cross-flow (Fig. 6) and the modified cross-flow arrangement (Fig. 7) for the $5 * 5$ nodes

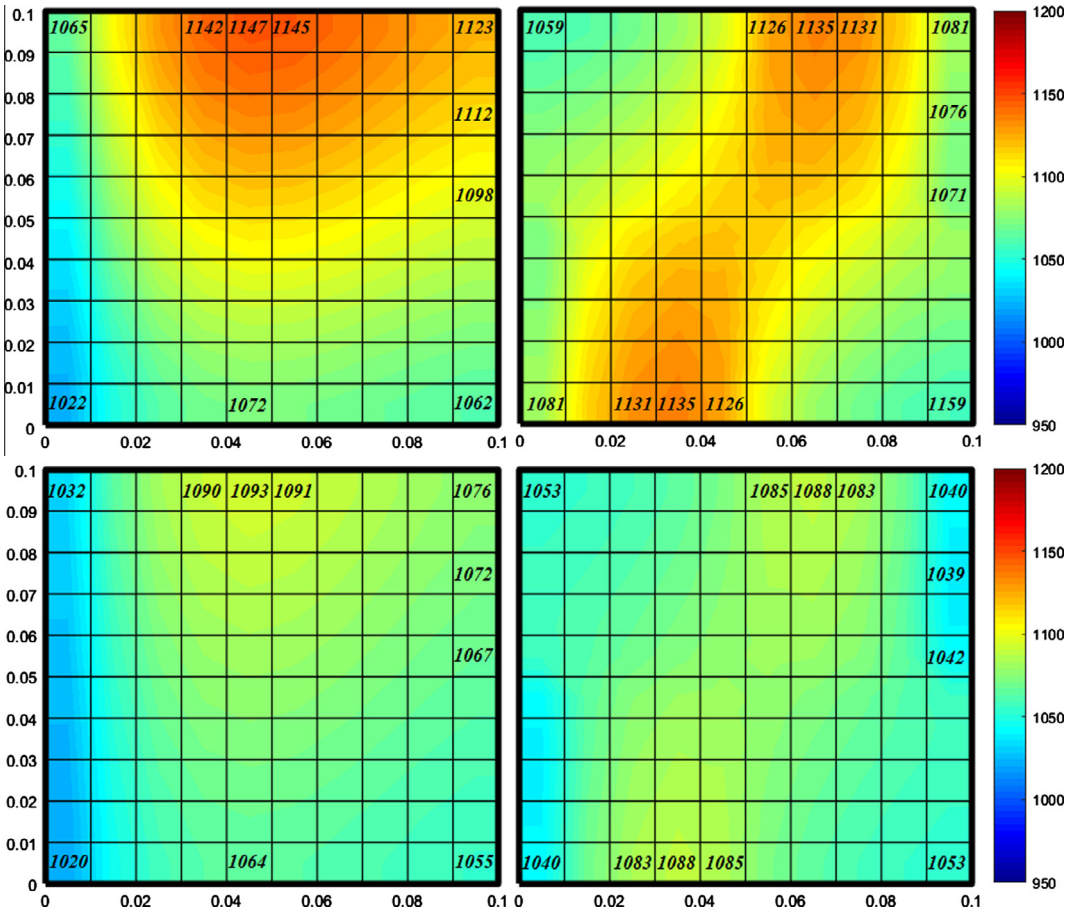

Fig. 5. Steady state nominal condition temperature profile. Top left: basic cross-flow. Top right: modified cross-flow. Bottom left: basic cross-flow with non-uniform air. Bottom right: modified cross-flow with non-uniform air.

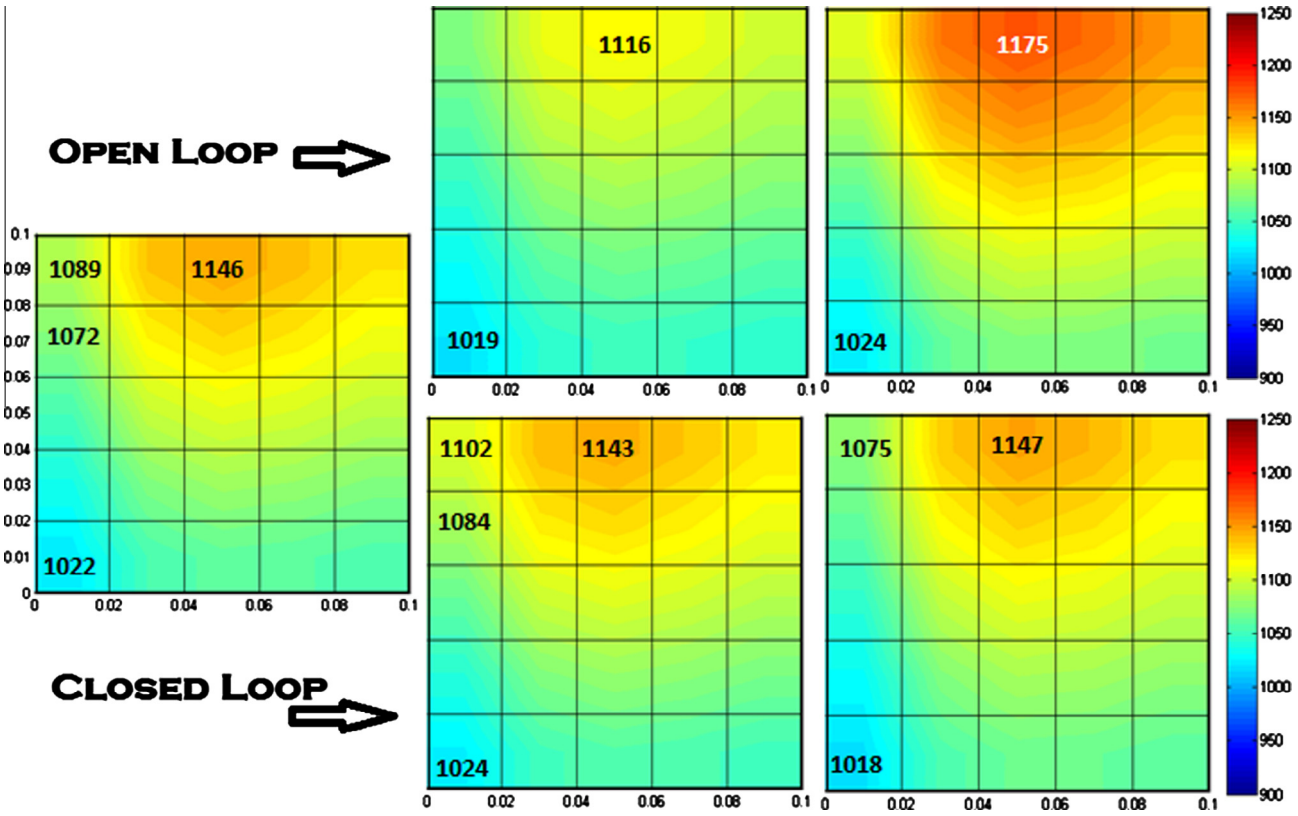

Fig. 6. Open loop (Top) and closed loop (Bottom) temperature profile for cross-flow. Single left plot: nominal condition, middle plots: power decreased by 15%, right plots: power increased by 15%.

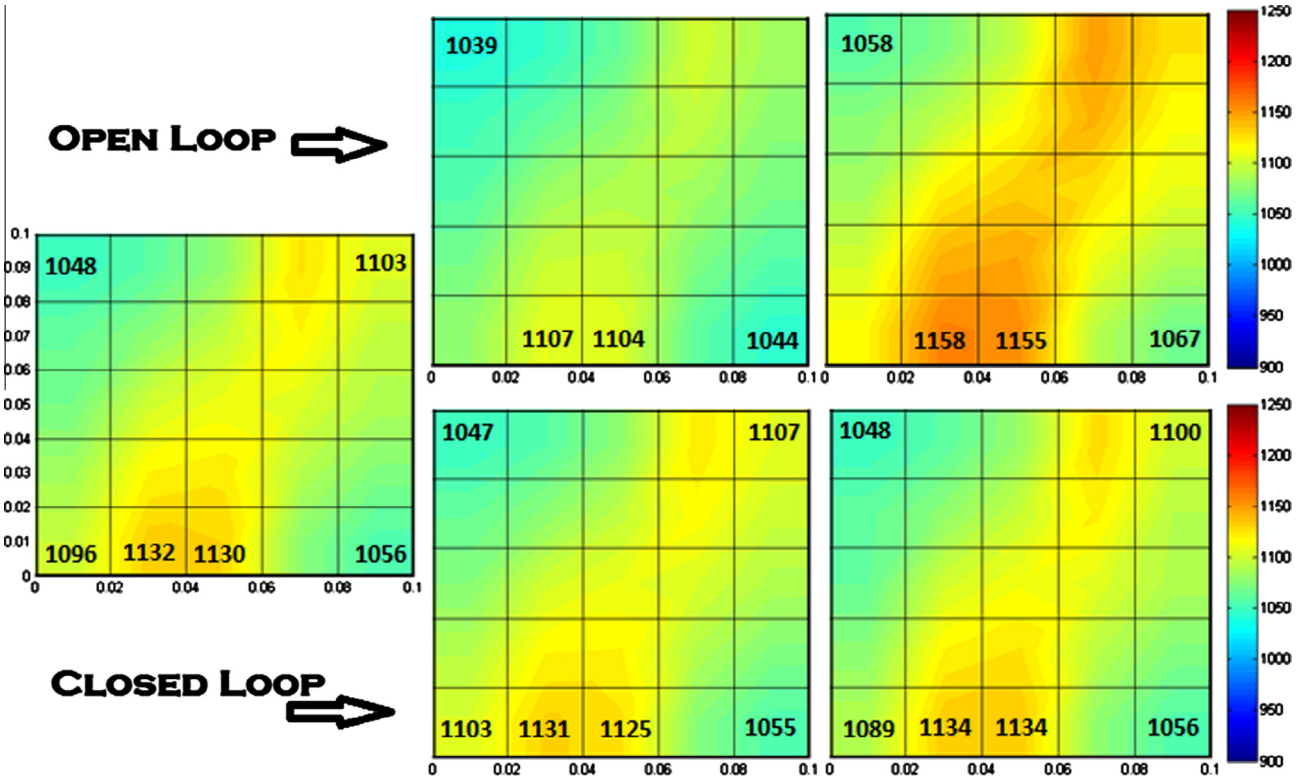

Fig. 7. Open loop (Top) and closed loop (Bottom) temperature profile for modified cross-flow. Single left plot: nominal condition, middle plots: power decreased by 15%, right plots: power increased by 15%.

model are discussed, for both open loop and closed loop temperature response during a load perturbation. The controller developed in Section 4 modulates the total air flow and the cathode inlet temperature in response to the changes in power demand. The load perturbation represents two step changes from the nominal operating condition. The first step, occurring at 1000 s, decreases output by 15% to 3 kW. The second step, occurring at 10,000 s, increases power by 15% from nominal power (or 33% from 3 kW) to 4 kW. Due to the large SOFC thermal mass, thermal dynamics are fairly slow. To make sure that there is no transients left, the step change is introduced after a significant period of time so that all variables are at the steady state value.

Fig. 6 illustrates both the open and closed loop temperature response to these step changes in power for the basic cross-flow configuration. Open loop temperature deviates a maximum of ±30 K from nominal operating conditions depending upon the spatial location. Areas downstream in the air flow direction and areas of high current, thus high temperature, deviate more than upstream low current areas. At peak power, the maximum temperature increases by 29 K from nominal. Essentially the hot areas get hotter (and colder) as power increases (and decreases). The closed loop response reduced these temperature fluctuations to less than 14 K.

With the same step changes in power applied to the modified cross-flow configuration, open loop temperature deviates up to ±26 K from the nominal conditions. The closed loop response of the modified cross-flow configuration leads to variations that are less than 7 K. The temperature profile of the modified cross-flow configuration, illustrated in Fig. 7, is not only more uniform under nominal operating conditions, but is also more responsive (controllable). Controllability Gramian and condition number are two analytical measures for controllability of a system. The modified cross flow arrangement had improved measures which is indicative of a more controllable system, i.e. the control methodology is more effective in minimizing temperature variations.

5.3. Temperature profile under load perturbation: non-uniform air flow rate

Fig. 5 illustrated how non-uniform air flow distribution among channels can be used to develop a more uniform temperature profile. Table 5 in the Appendix also demonstrates that non-uniform air flow distribution results in lower temperature gradients. STDEV in Table 5 denotes the standard deviations in temperature profile for each case. This section details both the open and closed loop response of the temperature profile when the air flow distribution is non-uniform. The control inputs (commands) are the inlet temperature and bulk air flow rate, with the distribution of air flow determined by the surface roughness factors of the channels.

Fig. 8 illustrates open loop and closed loop response for the basic cross-flow configuration with non-uniform air flow rate, while Fig. 9 illustrates the response of the modified cross-flow configuration. The step changes in power are the same as the previous section. Open loop temperature in Fig. 8 deviates ±26 K from the nominal condition (some nodes deviate as low as 3 K). The closed loop temperature response deviates less than 12 K from nominal. Both the open loop and closed loop response are modestly improved over the uniform flow case illustrated in Fig. 6.

The modified cross-flow configuration similarly benefits from a non-uniform air flow distribution as shown in Fig. 9. Open loop temperature deviates ±24 K from the nominal condition while closed loop temperature response deviates less than 6 K from nominal.

Comparing results of uniform air flow rate versus non-uniform ones, in Figs. 7 and 9, shows that non-uniform air flow rate for different channel results in more desirable temperature profile, and

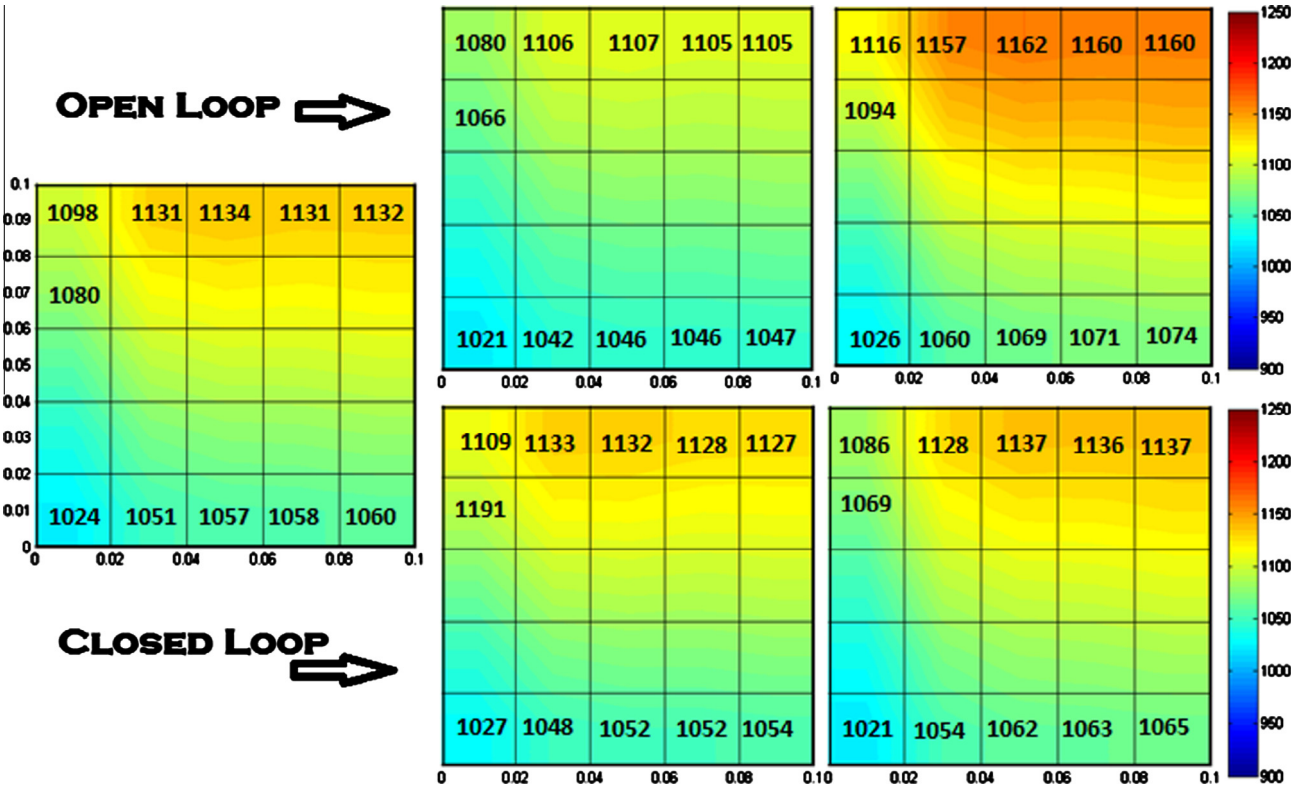

Fig. 8. Basic cross-flow with non-uniform air flow rate open loop and closed loop temperature profile. Single left plot: nominal condition, middle plots: power decreased by 15%, right plots: power increased by 15%.

lower temperature gradients. It also results in slightly lower temperature variation for open loop and the same temperature variations for closed loop for power variation of ±15% from nominal operating condition. Therefore, for closed loop operation is not as beneficial (recall that non uniform air has a modest but significant efficiency penalty.

Fig. 10 shows the actuator behavior during transient. The controller aims to minimize the overall temperature variations from nominal conditions, which leads to lowering the entire temperature profile by increasing air flow rate and decreasing cathode inlet temperature when power demand is increased from nominal condition. To find the air flow rate in each channel, one can multiply the air flow rate value from Fig. 10 by the ratios in the modified cross flow row of Table 4. Note that cathode inlet temperature is uniform across the channels.

6. Conclusions

Temperature gradients are a potentially limiting factor in the large scale commercial SOFC. Similarly, temperature perturbations are a potential limiting factor for application of SOFC for responsive power generation (i.e., power tracking). Here we discuss co-flow, counter-flow and cross-flow configurations. Numerical results

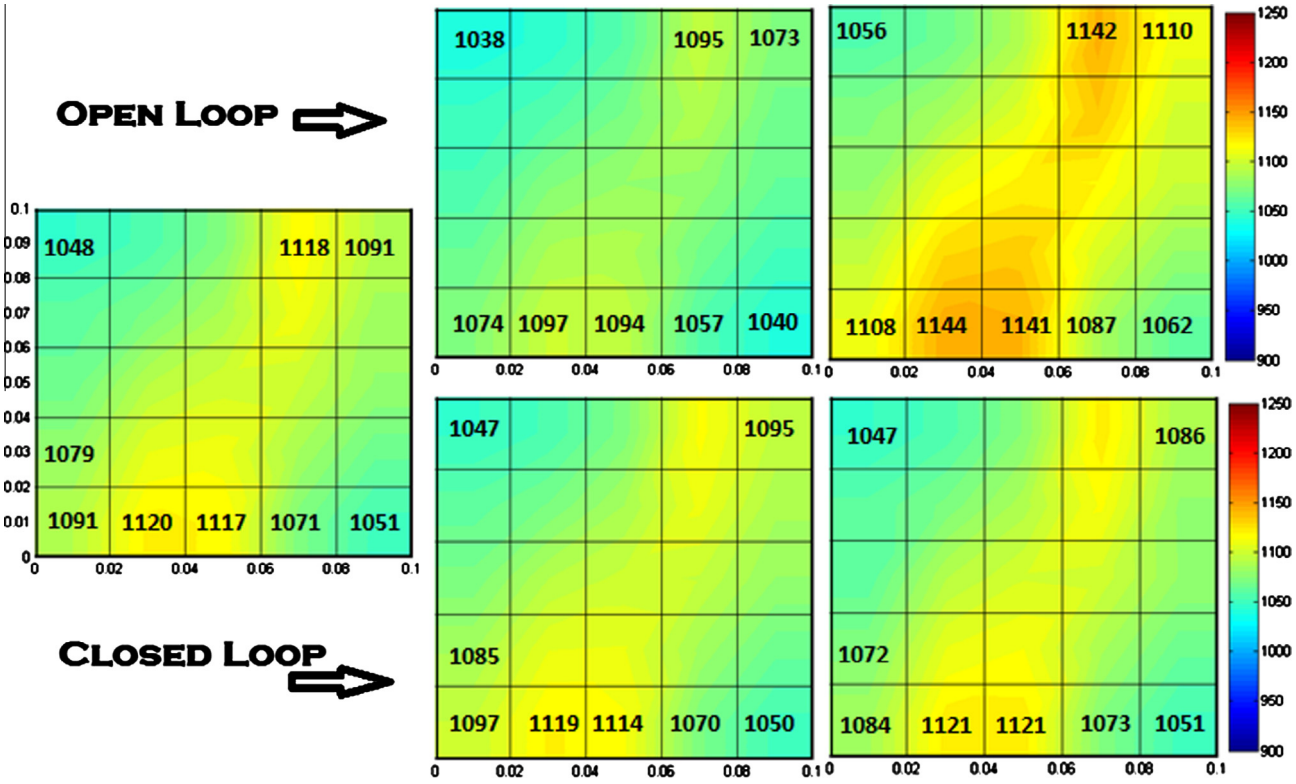

Fig. 9. Open loop (Top plots) and closed loop (Bottom plots) temperature profile for modified cross-flow with non-uniform air flow rate. Single left plot: nominal condition, middle plots: power decreased by 15%, right plots: power increased by 15%.

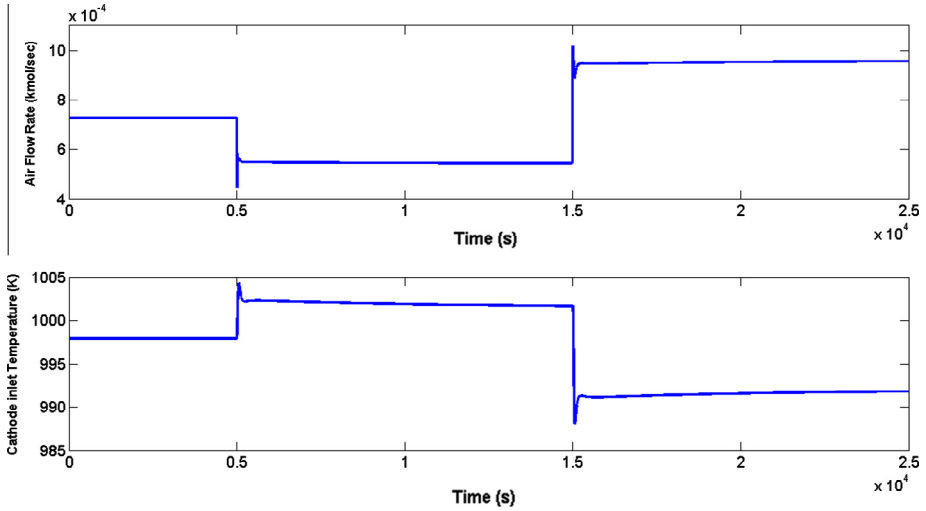

Fig. 10. Inputs during transients (Top: air flow rate. Bottom: cathode inlet temperature).

showed that temperature difference across the cell peaks at 100 K, 68 K, and 124 K for co-flow, counter-flow, and cross-flow, respectively. Counter-flow has the lowest peak temperature but higher temperature gradient in the high current region near the fuel entrance. For cross-flow SOFC, this paper analyzes three methods in which temperature profiles can be smoothed during steady and transient operations. Different cross-flow configurations were analyzed including the capability to differentiate the air flow rate between channels with surface roughness. Modified cross-flow results in lower temperature gradient (33 K versus 39 K), lower maximum temperature difference across the cell (76 K versus 124 K), e.g. more uniform temperature profile (Standard deviation of 22.5 versus 26.5), and higher efficiency (1.4%) than regular cross-flow arrangement at the expense of modest design modification. For open loop (and steady) operation, non-uniform air flow rate results in smoother temperature profile for both regular and modified cross-flow arrangements while decreasing efficiency. (Non uniform air flow results in 3% lower efficiency than the uniform flow rate for both cases.) As a result, the best temperature profile and gradient are through the use of modified flow and the non-uniform air flow at the same time, the latter one resulting in a modest efficiency loss (1.6% efficiency loss). Numerical simulations showed that for substantial power variations, ±15%, a high performance controller, modulating both air flow and inlet temperature, results in substantially lower temperature variations during transient response (14 K versus 27 K for regular cross flow). The modified cross-flow arrangement was more responsive to the controller (e.g., more controllable), resulting in a reduction of temperature perturbations by 75% (7 K versus 27 K). In all cases, both steady and transient, the modified cross-flow configuration outperformed the basic cross-flow configuration. Similarly, in all open loop cases the non-uniform distribution of air flow reduced temperature variations as well as the gradients and maximum temperature across the cell, at the cost of a modest increase in the fuel flow rate (and thus a small decrease in the overall efficiency). These general trends hold for the closed loop operation, though the improvement due to non-uniform air flow is minimal since the modified cross-flow is more controllable.

Table 1
Nominal SOFC operating condition for 10 × 10 nodes model.

Parameter	Nominal value
Net power	3.5 kW
Fuel utilization	0.85
Cathode inlet temperature	1021 K
Air flow rate	$86 * 10^{-5}$ kmol/s
Anode inlet temperature	600 K

Table 2
Nominal SOFC operating condition for 5 × 5 nodes model.

Parameter	Nominal value
Net power	3.5 kW
Fuel utilization	0.85
Cathode inlet temperature	998 K
Air flow rate	$73 * 10^{-5}$ kmol/s
Anode inlet temperature	600 K

Table 3
Disturbances, actuator and sensors applied to the linear model and control development.

Disturbances (D_i)	(1) Fuel cell power
Actuators (A_i)	(1) Cathode inlet temperature
	(2) Air flow rate
Sensors (S_i)	(1) Current
	(2) Plate temperature of 1st node
	(3) Plate temperature of 3rd node
	(4) Plate temperature of 5th node
	(5) Plate temperature of 7th node
	(6) Plate temperature of 9th node
	(7) Plate temperature of 11th node
	(8) Plate temperature of 13th node
	(9) Plate temperature of 15th node
	(10) Plate temperature of 17th node
	(11) Plate temperature of 19th node
	(12) Plate temperature of 21st node
	(13) Plate temperature of 23rd node
	(14) Plate temperature of 25th node
	(15) Fuel flow rate
Control variables (CV_i)	(i) *i*th node electrolyte temperature

Acknowledgement

This work is funded by the National Science Foundation grant CMMI-141583.

Appendix A

See Tables 1–5.

Table 4
Ratio of total mass flow in each channel in non-uniform air flow distributions in regular and modifies cross-flow configurations, 5 nodes model.

	Channel 1	Channel 2	Channel 3	Channel 4	Channel 5
Regular cross-flow	0.1	0.25	0.25	0.25	0.15
Modified cross-flow	0.25	0.2	0.25	0.1	0.2

Table 5
Maximum temperature gradient, maximum temperature difference across the cell, fuel flow rate and standard deviation for temperature profile for three different flow arrangements for 10 × 10 nodes models.

	Max temp gradient	Max temp difference across the cell	Fuel flow rate	STDEV
Cross-flow	39	124	3.62E−5	26.5
Cross-flow with non-uniform air	31.7	73	3.73E−5	10
Dir 4	37.8	70	3.56 E−5	10.7
Dir 4 non-uniform air	27	45	3.71 E−5	6.8
Modified cross-flow	33	76	3.57E−5	22.5
Modified cross-flow with non-uniform air	28	49	3.68E−5	8.86

References

[1] Kind P. Energy infrastructure advocates. Disruptive challenges: financial implications and strategic responses to a changing retail electric business. <http://www.eei.org/ourissues/finance/documents/disruptivechallenges.pdf>.

[2] Corneli S. Distributed energy resources and the "Utility Death Spiral" what it is why it is happening what to do (and not do) about it. <http://www.jisea.org/pdfs/2014_annual_meeting_corneli.pdf>.

[3] Yan J, Chou SK, Desideri U, Xia X. Innovative and sustainable solutions of clean energy technologies and policies (Part I). Appl Energy 2014;130:447–9.

[4] Komatsu Y, Brus G, Kimijima S, Szmyd JS. The effect of over potentials on the transient response of the 300W SOFC cell stack voltage. Appl Energy 2014;115:352–9.

[5] Iora P, Silva P. Innovative combined heat and power system based on a double shaft intercooled externally fired gas cycle. Appl Energy 2013;105:108–15.

[6] IEEE survey of experts. Power systems of the future: the case for energy storage, distributed generation, and microgrids. <http://smartgrid.ieee.org/images/features/smart_grid_survey.pdf>.

[7] Lo C, Ansar N. Alleviating solar energy congestion in the distribution grid via smart metering communications. IEEE Trans Parall Distrib Syst 2012;23(9).

[8] Viral R, Khatod DK. Optimal planning of distributed generation systems in distribution system: a review. Renew Sustain Energy Rev 2012;16(7):5146–65.

[9] Zhao L, Brouwer J, Liu J, James S, Siegler J, Kansal A, et al. Fuel cells for data centers: power generation inches from the server. Microsoft research technical report MSR-TR-2014-37. <http://research.microsoft.com/pubs/210641/FCDC-TechReport.pdf>.

[10] Smart grid system report, report to congress August 2014, United States Department of Energy; 2014. <https://www.smartgrid.gov/sites/default/files/doc/files/2014-Smart-Grid-System-Report.pdf>.

[11] Narula K, Nagai Y, Pachauri S. The role of decentralized distributed generation in achieving universal rural electrification in South Asia by 2030. Energy Policy 2012;47(August):345–57.

[12] Buonomano A, Calise F, Ferruzzi G, Palombo A. Molten carbonate fuel cell: an experimental analysis of a 1 kW system fed by landfill gas. Appl Energy 2015;140(15):146–60.

[13] Bove R, Lunghi P. Experimental comparison of MCFC performance using three different biogas types and methane. J Power Sources 2005;145(2):588–93.

[14] Cigolotti V, McPhail S, Moreno A, Yoon SP, Han JH, Nam SW, et al. MCFC fed with biogas: experimental investigation of sulphur poisoning using impedance spectroscopy. Int J Hydrogen Energy 2011;36(16):10311–8.

[15] Mueller F, Jabbari F, Gaynor R, Brouwer J. Novel solid oxide fuel cell system controller for rapid load following. J Power Sources 2007;172(1):308–23.

[16] Mueller F, Tarroja B, Maclay J, Jabbari F, Brouwer J, Samuelsen S. Design, simulation and control of a 100 Megawatt class solid oxide fuel cell gas turbine hybrid system. Denver (Colorado): ASME; 2008.

[17] Murshed AM, Huang B, Nandakumar K. Estimation and control of solid oxide fuel cell system. Comput Chem Eng 2010;34(1):96–111.

[18] Mueller F, Jabbari F, Brouwer J, Roberts R, Junker T, Ghezel-Ayagh H. Control design for a bottoming solid oxide fuel cell gas turbine hybrid system. J Fuel Cell Sci Technol 2007;4:221–30.

[19] Stiller C, Thorud B, Bolland O, Kandepu R, Imsland L. Control strategy for a solid oxide fuel cell and gas turbine hybrid system. J Power Sources 2006;158(1):303–15.

[20] Sorce A, Greco A, Magistri L, Costamagna P. FDI oriented modeling of an experimental SOFC system, model validation and simulation of faulty states. Appl Energy 2014;136:894–908.

[21] Ferrari ML. Advanced control approach for hybrid systems based on solid oxide fuel Cells. Appl Energy 2015;145:364–73.

[22] Barelli L, Bidini G, Ottaviano A. Part load operation of a SOFC/GT hybrid system: dynamic analysis. Appl Energy 2013;110:173–89.

[23] Zaccaria V, Tucker D, Traverso A. Transfer function development for SOFC/GT hybrid systems control using cold air bypass. Appl Energy 2016;165:695–706.

[24] Singh P, Bansal NP. Advances in solid oxide fuel cells VI: Ceramic engineering and science proceedings, vol. 31(4). John Wiley & Sons; 2010 [November 23].

[25] Zhang H, Zhang W, Lu Z, Weng S. Performance comparison on cross-flow and counter-flow planar solid oxide fuel cell. In: Proceedings of ASME turbo expo 2012 GT2012 June 11–15, 2012, Copenhagen, Denmark.

[26] Colpan C Ozgur, Hamdullahpur F, Dincer F. Transient heat transfer modeling of a solid oxide fuel cell operating with humidified hydrogen. In: Proceedings of the international conference on hydrogen production, June 16e18, 2010, Istanbul, Turkey.

[27] Aguiar P, Adjiman CS, Brandon NP. Anode-supported intermediate temperature direct internal reforming solid oxide fuel cell. I: Model-based steady-state performance. J Power Sources 2004;138(1–2):120–36.

[28] ŞEN F. Thermal management of solid oxide fuel cells by flow arrangement [Master]. Middle East Technical University; 2012.

[29] Yuan P, Liu SF. Numerical analysis of temperature and current density distribution of a planar solid oxide fuel cell unit with nonuniform inlet flow. Numer Heat Transf Part A 2007;51:941–57.

[30] Mueller F, Gaynor R, Auld AE, Brouwer J, Jabbari F, Samuelsen GS. Synergistic integration of a gas turbine and solid oxide fuel cell for improved transient capability. J Power Sources 2008;176(1):229–39.

[31] Mueller F. On the intrinsic transient capability and limitations of solid oxide fuel cell systems. J Power Sources 2009;187(2):452–60.

[32] Yang J, Li X, Mou H-G, Jian L. Predictive control of solid oxide fuel cell based on an improved Takagi-Sugeno fuzzy model. J Power Sources 2009;193(2):699–705.

[33] Yang J, Li X, Mou H-G, Jian L. Control-oriented thermal management of solid oxide fuel cells based on a modified Takagi-Sugeno fuzzy model. J Power Sources 2009;188(2):475–82.

[34] Mueller F. Design and simulation of a tubular solid oxide fuel cell system control strategy [Master]. Irvine: University of California, Irvine; 2005.

[35] Fardadi M, McLarty DF, Jabbari F. Controlling spatial temperature variation in a rapid load following SOFC. In: The ASME 2013 11th international fuel cell science, engineering & technology conference, June 14–16, 2013, Minneapolis, MN.

[36] Haberman BA, Young JB. Numerical investigation of the air flow through a bundle of IP-SOFC modules. Int J Heat Mass Transf 2005;48(25–26):5475–87.

[37] Park H-K, Lee Y-R, Kim M-H, Chung G-Y, Nam S-W, Hong S-A, et al. Studies of the effects of the reformer in an internal-reforming molten carbonate fuel cell by mathematical modeling. J Power Sources 2002;104(1):140–7.

[38] Li P-W, Chyu MK. Simulation of the chemical/electrochemical reactions and heat/mass transfer for a tubular SOFC in a stack. J Power Sources 2003;124(2):487–98.

[39] Tucker D, VanOsdol J, Liese E, Lawson L, Zitney S, Gemmen R, et al. Evaluation of methods for thermal management in a coal-based SOFC turbine hybrid through numerical simulation. J Fuel Cell Sci Technol 2012;9(4):9 [041004].

[40] Nakajo A, Wuillemin Z, Van herle J, Favrat D. Simulation of thermal stresses in anode-supported solid oxide fuel cell stacks. Part I: Probability of failure of the cells. J Power Sources 2009;193(1):203–15.

[41] Nakajo A, Wuillemin Z, Van herle J, Favrat D. Simulation of thermal stresses in anode-supported solid oxide fuel cell stacks. Part II: Loss of gas-tightness, electrical contact and thermal buckling. J Power Sources 2009;193(1):216–26.

[42] Inui Y, Ito N, Nakajima T, Urata A. Analytical investigation on cell temperature control method of planar solid oxide fuel cell. Energy Convers Manage 2006;47(15–16):2319–28.

[43] Bavarian M, Soroush M. Steady-state multiplicity in a solid oxide fuel cell: practical considerations. Chem Eng Sci 2012;67(1):2–14 [Dynamics, control and optimization of energy systems].

[44] Bavarian M, Soroush M. Mathematical modeling and steady-state analysis of a proton-conducting solid oxide fuel cell. J Process Control 2012;22(8):1521–30.

[45] Christman KL, Jensen MK. Solid oxide fuel cell performance with cross-flow roughness. J Fuel Cell Sci Technol 2011;8(April):024501.

[46] Recknagle KP, Williford RE, Chick LA, Rector DR, Khaleel MA. Three-dimensional thermo-fluid electrochemical modeling of planar SOFC stacks. J Power Sources 2003;113(1):109–14.

[47] Chen D, Zeng Q, Su S, Bi W, Ren Z. Geometric optimization of a 10-cell modular planar solid oxide fuel cell stack manifold. Appl Energy 2013;112:1100–7.

[48] Razbani O, Wærnhus I, Assadi M. Experimental investigation of temperature distribution over a planar solid oxide fuel cell. Appl Energy 2013;105:155–60.

[49] Iwata M, Hikosaka T, Morita M, Iwanari T, Ito K, Onda K, et al. Performance analysis of planar-type unit SOFC considering current and temperature distributions. Solid State Ionics 2000;132:297–308.

[50] Fardadi M, Mueller F, Jabbari F. Feedback control of solid oxide fuel cell spatial temperature variation. J Power Sources 2010;195(13):4222–33.

[51] Fardadi M, McLarty D, Jabbari F. Actuator imperfections in spatial temperature control of SOFC. ASME J Fuel Cell Sci Technol 2013;10(June):031005.

[52] Fardadi M. High performance control methods to reduce spatial temperature transients in emerging energy systems [Doctorate]. Irvine: University of California, Irvine; 2013.

[53] Fardadi M, McLarty DF, Brouwer J, Jabbari F. Enhanced performance of counter-flow SOFC with partial internal reformation. Int J Hydrogen Energy 2014;39(34):19753–66.

[54] McLarty D. Thermodynamic modeling and dispatch of distributed energy technologies including fuel cell – gas turbine hybrids [Doctorate]. Irvine: University of California, Irvine; 2013.

[55] Mueller F. The dynamics and control of integrated solid oxide fuel cell systems: transient load-following and fuel disturbance rejection [Doctorate]. Irvine: University of California, Irvine; 2008.

[56] Chalk S. American recovery and reinvestment act program plan for the office of energy efficiency and renewable energy. Department of Energy, The Office of Energy Efficiency and Renewable Energy (EERE); 2009.

[57] Sison-Lebrilla E, Kibrya G, Tiangco V, Yen D, Sethi P, Kane M. Research development and demonstration roadmap. In: PIER renewable energy technologies program. Sacremento: California Energy Commission; 2007. p. 45 [August].

[58] Williams MC, Strakey JP, Surdoval WA, Wilson LC. Solid oxide fuel cell technology development in the US. Solid State Ionics 2006;177(19e25):2039–44.

[59] Serincan MF, Pasaogullari U, Sammes NM. A transient analysis of a micro-tubular solid oxide fuel cell (SOFC). J Power Sources 2009;194(2):864–72.

[60] Nakajo A, Stiller C, Harkegard G, Bolland O. Modeling of thermal stresses and probability of survival of tubular SOFC. J Power Sources 2006;158(1):287–94.

[61] Aguiar P, Adjiman CS, Brandon NP. Anode-supported intermediate-temperature direct internal reforming solid oxide fuel cell: II. Model-based dynamic performance and control. J. Power Sources 2005;147:136–47.

[62] Zhou K, Doyle JC. Essentials of robust control. Prentice Hall; 1998.
[63] Boyd S, Ghaoui LE, Feron E, Balakrishnan V. Linear matrix inequalities in system and control theory; 1994.
[64] Gahinet P, Apkarian P. A linear matrix inequality approach to H-infinity control. Int J Robust Nonlinear Contr 1994;4(4):421–48.
[65] Scherer C, Gahinet P, Chilali M. Multi objective output-feedback control via LMI optimization. IEEE Trans Automat Contr 1997;42(7):896–911.
[66] Skelton RE, Iwaskai T, Grigoriadis K. A unified algebraic approach to linear control design. London: Taylor and Francis; 1998.